Three-Dimensional Unsteady Flow in an Axial Flow Turbine

O. P. Sharma* and T. L. Butler†
Pratt & Whitney—Engineering Division, East Hartford, Connecticut
and
H. D. Joslyn‡ and R. P. Dring§
United Technologies Research Center, East Hartford, Connecticut

The results of an experimental program directed at understanding the unsteady mean and turbulent flow in a large-scale 1-½ stage research turbine are presented. High response instrumentation and the phase-locked averaging data reduction technique were utilized to acquire data having high spatial and temporal resolution. These data included the unsteady three-dimensional distribution of mean and turbulent velocities and total and static pressures. The data between the guide vane and the rotor and downstream of the rotor are presented herein. The flow downstream of the vane was found to be essentially steady and was dominated by large Reynolds stresses in the wakes and secondary flow regions. In contrast, the flow downstream of the rotor was highly unsteady. Two different rotor exit flow regimes were identified, corresponding to maximum and minimum interaction of the rotor leading edges with the upstream vane wakes. During the maximum interaction, the vane wakes merged with the rotor wakes, the midchannel flow was fairly uniform, and two strong secondary flow vortices were present. During minimum interaction, the vane wakes entered the rotor passages between airfoils, the midchannel flow was nonuniform, and the secondary flow vortices were less well defined.

Nomenclature

bx	= airfoil axial chord
C	= total velocity magnitude
C_{PT}	= total pressure coefficient, $= -(P_{to} - P_t)/\frac{1}{2}\rho U_B^2$
C_{PS}	= static pressure coefficient, $= -(P_0 - P)/\frac{1}{2}\rho U_B^2$
Cx	= axial throughflow velocity at inlet
$F(t)$	= phase-locked ensemble average of flow quantity F
F'	= instantaneous value of flow quantity F
q^2	= turbulence intensity, $= u^2 + v^2 + w^2$
P_0, P_{to}	= static and total pressure at turbine inlet
R	= radius
U	= streamwise (meanline direction) velocity component
U_B	= rotor speed at midspan
V	= velocity component normal to streamwise direction in the axial tangential plane
W	= velocity component in the radial direction
u^2, v^2, w^2	= streamwise, normal, and radial components of turbulence intensity
uv, uw, vw	= Reynolds shear stress components
α	= pitch angle, $= \sin^{-1}(W/C)$
β	= yaw angle, $= \sin^{-1}[V/(C\cos\alpha)]$

Presented as Paper 83-1170 at the AIAA/SAE/ASME 19th Joint Propulsion Conference, Seattle, Wash., June 27-29, 1983; received Oct. 4, 1983; revision submitted Oct. 1984.

*Project Engineer. Member AIAA.
†Senior Engineer.
‡Research Engineer.
§Manager, Gas Turbine Technology. Member AIAA.

Introduction

ALTHOUGH aircraft gas turbine designers realize that the flowfield in a real turbine environment is highly unsteady and three-dimensional, they are forced to rely on streamline curvature flow solvers and two-dimensional, steady analytical calculation methods to carry out design studies. Streamline curvature methods are used to define the spanwise variation in velocity triangles for a particular row of blades. For these given velocity triangles and inlet and exit flow conditions, potential or Euler flow solvers are used to define the airfoil geometry and pressure distribution on the airfoil surfaces. Two-dimensional boundary-layer calculations are then conducted to estimate the magnitude of profile losses associated with each airfoil section. Estimates of endwall and tip clearance secondary losses are obtained from empirical correlations derived from the available stationary cascade data base. Application of these loss components to realistic turbines results in significant overestimation of performance. This is not surprising, since these loss-estimation methods do not explicitly account for the three-dimensional and unsteady nature of the flowfield in the actual turbine. Because realistic models of the loss generation mechanisms in the unsteady flow environment are unavailable, the designers are forced to use multiplication factors that, when applied to the cascade correlations, give reasonably good estimates of losses in turbines. These factors can be large; e.g., Dunham and Came[1] chose to multiply their cascade endwall loss correlation by a factor of 2.4 in order to obtain realistic performance estimates of rotating turbine rigs. It is unlikely that these factors reflect the true physical nature of the loss generation mechanisms in the unsteady environment and, therefore, can result in design of a turbine at a nonoptimal configuration. It should be pointed out, however, that substantial improvements in uncooled gas turbine performance have been achieved over the past 15 years in parallel with the development of these two-dimensional viscous and invisid calculation procedures. Admittedly, it would be difficult to distinguish between the relative contribution of the improved calculation methods,

the large number of development tests, and the ingenuity of the turbine designers in achieving these improved turbine performance levels.

From the above discussion it is apparent that improved analytical models of the loss generation mechanisms in unsteady flows would provide increased understanding of the turbine flowfield and would lead to improved gas turbine engine performance. It would be highly desirable to have a purely analytical basis for these unsteady loss generation models; however, even in the steady flow environment, profile loss calculation methods rely on semiempirical turbulence models to allow calculation of transitional and turbulent boundary-layer flows on turbine airfoils. Thus, the availability of data that provide some clues about the loss generation mechanisms in the unsteady environment would be a first step toward developing realistic loss models for the turbine design application.

A number of studies in the literature provide data obtained in an unsteady environment for isolated airfoils and compressors.[2-6] Unfortunately, boundary layers on turbine airfoils develop under favorable pressure gradients and at Reynolds numbers where transition from laminar to turbulent flow is a primary factor in controlling the growth of loss. The location of transition in accelerating flowfields is strongly dependent on the nature and magnitude of disturbances produced by the unsteady flowfield. Errors in the estimation of the transition point on a turbine airfoil can result in much higher inaccuracies in the magnitude of calculated losses than for a compressor airfoil. This is because transition on compressor airfoils is normally caused by laminar separation, which is easier to locate. Therefore one would expect significant differences in the turbine flowfield as compared to an isolated airfoil or compressor in the unsteady flow environment. Pfeil and his co-workers[7,8] have recently published results of experiments where they studied the development of boundary layers under almost zero pressure gradient which were influenced by periodically unsteady wakes generated from rotating rods upstream of the test plate. They showed that the boundary-layer development varied significantly depending on whether the plate was inside or outside the wakes, principally because of the movement of the location of transition.

A number of three-dimensional calculation procedures[9-12] have been developed over the past few years which, until now, have had only limited success in predicting the complex three-dimensional flowfield even for linear cascades. Since most of these calculation methods rely on empirical turbulence models to predict the viscous flowfield, any experimental information about the distribution of turbulence in the flowfield would prove useful to the developers. Although detailed experimental data are available for linear cascade flows from the benchmark quality tests conducted by Langston et al.[13] Marchal and Sieverding[14] and others, these data are limited to mean flow quantities. At present, relatively little information is available about the nature of turbulence in the turbine passage.

This paper presents some of the data obtained from an investigation that was conducted to obtain detailed information about the unsteady, three-dimensional mean, and turbulent flowfield between the blade rows of a large scale, low speed, 1½ stage axial flow research turbine. A brief description of the test facility, instrumentation, and data acquisition system is given in the following section.

Experimental Setup, Instrumentation, and Data Reduction

The experimental program was conducted at the United Technologies Research Center in the 5-ft-diam large-scale rotating rig (LSRR). The LSRR is a large-scale, low-speed rotating wind tunnel that can be used to simulate the flowfield in axial flow turbomachines. A detailed description of the test facility, instrumentation, and computer-controlled on-line data acquisition system is given by Joslyn et al.[15] For the purpose of the present program, the tunnel was assembled in a 1½ stage axial flow turbine configuration, representing the first three blade rows of the high-pressure turbine of a typical high bypass ratio aircraft gas turbine engine. A schematic of the test rig is shown in Fig. 1, and the relevant geometric and aerodynamic parameters are provided in Table 1. Data were acquired at the four axial stations shown in Fig. 1. A three element hot-film probe was used to measure the velocity field and an aerodynamically shielded high response pressure transducer was used to measure the total pressure field. The probes were chosen so that their size was small relative to the physical dimensions of the flow. For example, the sensing volume of the three-sensor hot-film probe was 1/15 of the inlet guide vane wake width at midspan.

An extensive amount of data had been obtained in this facility using pneumatic instrumentation for both the flowfield at the four axial stations and on the airfoil surfaces.[16,17] The primary objective of the present program was to identify the details of the mean and the turbulent flow in the unsteady environment. Thus the data were acquired at approximately 1000 locations at each axial station in order to capture the spatial details of the flowfield over two first vane pitches. At each location 100 timewise data points were acquired corresponding to 100 different positions of one rotor blade passage relative to the measurement location. This was repeated for three successive rotor blade passings. This timewise sequence of data acquisition was repeated once per revolution for 100 successive revolutions. A rotor blade activated trigger mechanism was used to ensure that all 100 timewise data acquistions were in phase. Thus, approximately 180 million measurements were made at each of the four axial stations.

These data, which were stored in digital form as voltages on magnetic tape, consisted of three signals of voltage output from the hot-film sensors, a signal obtained at the same time from a probe-mounted thermocouple, and two voltage signals representing total pressure from the shielded pressure transducer and the output from a second probe-mounted thermocouple. These instantaneous data where converted into engineering units using calibration systems for the hot-film probe and the pressure transducer. A new three-sensor hot-wire data reduction system, described by Butler and Wagner,[18] was developed to ensure accurate conversion of instantaneous digitized voltage signals to the three orthogonal components of velocity. These engineering unit data consisted of three orthogonal components of velocity and total pressure and were reduced in number using the signal enhancement technique commonly known as the phase-locked averaged (PLA) method.

The phase-locked averaged mean velocity and total pressure were combined to obtain a measure of the static pressure. The total pressure probe size and the flow speed define a time scale for the deceleration of an unsteady streamline which stagnates

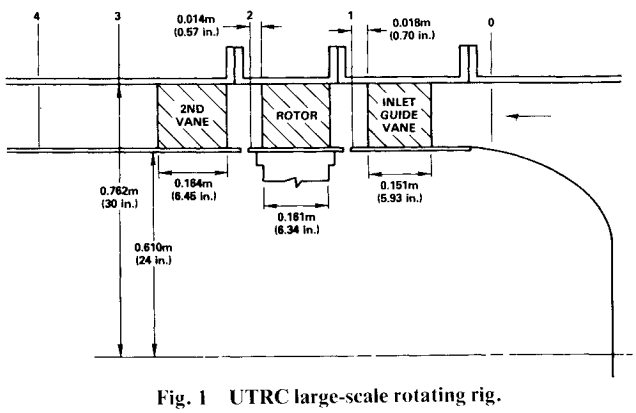

Fig. 1 UTRC large-scale rotating rig.

against the transducer diaphragm. For the conditions of this experiment, this time scale is about forty times smaller than the time scale associated with the blade-to-blade unsteadiness. Thus, ignoring small-scale unsteadiness, the stagnation process can be considered quasisteady, and Bernoulli's equation gives a good estimate of static pressure in terms of the total pressure and velocity.

$$P = P_{to} - \tfrac{1}{2}\rho C^2 \tag{1}$$

Because the velocity and total pressure measurements are made at different times, a reliable measure of the fluctuating static pressure cannot be made using the technique. Thus, the phase-locked ensemble averaged velocities and total pressure were combined to yield a phase-locked ensemble averaged static pressure. Static pressure data are reported in Ref. 30.

Although a number of investigators have used the PLA technique in unsteady flows, some confusion does exist concerning the correct application of this technique for measuring flow in turbomachinery. For this reason, in the following subsection some comments are made to help clear up this confusion.

Phase-Locked Averaging Technique

Data obtained in highly unsteady flow environments using high response instrumentation must be reduced by using some signal enhancement technique to identify separately the magnitude of mean quantities and disturbances. The disturbances on the mean flow are normally of two kinds. The first is associated with the randomness of the flow velocities, and are usually identified as turbulence. The second kind of disturbance is periodic in nature, and occurs because of blade-to-blade flow effects. The inviscid part of this disturbance can be calculated by using existing potential and Euler flow solvers. The viscous part of this disturbance appears as wakes and vortices in the turbomachine passages. The periodic disturbances always appear at discrete frequencies, whereas the random disturbances have energies distributed over a wide range of frequencies. The turbine designer is interested in both types of disturbances. The structure of the random disturbances control the distribution of turbulence which in turn influences both heat transfer and loss growth on turbine airfoils. The periodic disturbances set up unsteady flows that influence the interactions with adjoining blade rows.

The concepts of PLA are described by Gostelow,[19] although Hill and Railly[20] may have been the first investigators to apply the PLA technique to measure velocities downstream of a rotating machine. Lakshminarayana et al.[21,22] have used this technique extensively in obtaining detailed mean and turbulence flow data in compressors. Because of the large quantities of data which must be acquired to adequately define the flowfield for unsteady turbomachinery applications, many investigators have assumed that the hot wire output voltage is linearly related to the flow velocity and have used conditional averaged voltages to deduce the velocity. This relationship is truly linear only if the flow is one-dimensional, the hot-wire sensor is optimally oriented to the flow direction, and linearizing circuitry is used. However, turbomachinery flows are highly unsteady and three-dimensional, resulting in significant variations in velocity magnitude and direction relative to the sensor during the period that data are being acquired. The use of averaged voltage outputs to deduce average velocity under these conditions can result in large errors. In the present program, the instantaneous output voltages from the three element hot-film probes were reduced to three instantaneous orthogonal components of velocity. At each fixed probe location, 300 timewise values of each velocity component and total pressure were measured and reduced to engineering units ($t = 1$-300). The tth value for each of the four quantities was then ensemble averaged over 100 revolutions to obtain the PLA velocity:

$$F(t) = 1/100 \sum_{n=1}^{100} F(t) \tag{2}$$

The turbulent stresses were then calculated by using instantaneous and PLA velocities as follows:

$$\overline{(vi\ vj)}_t = 1/100 \sum_{n=1}^{100} (V'iV'j - ViVj)_t \tag{3}$$

where vi, vj are PLA turbulent stress in i-j plane, and i, j are velocity components in i and j directions.

Using this data processing method, each measurement location contained 300 values (representing timewise values for three airfoil passages) of the three components of the PLA velocity, the six components of Reynolds stresses, and the total and static pressures. These processed data were further reduced to define time average (averaged over 300 values to filter out the effect of the presence of rotor) and disturbance quantities as follows:

$$F = 1/300 \sum_{t=1}^{300} F(t) \tag{4}$$

$$fifj = 1/300 \sum_{t=1}^{300} [FiFj - Fi(t)Fj(t)] \tag{5}$$

where F is the time averaged value of flow quantity $F(t)$ and $fifj$ is the disturbance value due to the presence of unsteadiness generated by the rotor.

Table 1 Aerodynamic and geometric parameters for LSRR

Throughflow velocity, Cx	= 19 m/s (75 ft/s)		
Inlet total pressure	= ambient, 1 atm		
Inlet total temperature	= ambient, −294 K (530°R)		
Flow coefficient, Cx/U_B	= 0.78		
	Guide vane	Rotor	Second vane
Axial chord, bx	0.151 m (5.93 in.)	0.161 m (6.34 in.)	0.164 m (6.45 in.)
Number of airfoils	22	28	28
Aspect ratio S/bx	1.01	0.946	0.930
Interairfoil gap	$0.65(bx)$	$0.56(bx)$	
Tip clearance		$0.01(bx)$	
Midspan inlet metal angle	90 deg	42 deg	46 deg
Midspan exit metal angle	21 deg	26 deg	25 deg
Exit velocity, absolute frame	64 m/s (210 ft/s)	34 m/s (112 ft/s)	50 m/s (165 ft/s)
Exit Re No./in	1.09×10^5	1.04×10^5	0.86×10^5

These time-averaged and disturbance values were made available, along with the 300 values of PLA data at each measurement location, in the form of a large computer data file. A software package was written to allow the data to be plotted on the measurement window at each measurement station, allowing the flowfield to be reviewed as it is influenced by the movement of the rotor. Some of the data obtained downstream of the first vane and the rotor are shown in the following two sections. Data obtained downstream of the second vane will be presented at a later date.

Vane Exit Flow

The development of secondary flow in a turning cascade of airfoils is strongly dependent on the inlet boundary layer as shown by Squire and Winter[23] and by Hawthorne and his coworkers.[24] The inlet flow to this vane (station 0) is fairly uniform, and the turbulence intensity in the main stream is of the order of about 0.8-1%. Measurements of the total pressure profile at station 0 (Fig. 1) had previously indicated that the boundary-layer thicknesses were of the order of about 5% of the span at the root and about 8% of the span at the tip.

A review of the unsteady data obtained at station 1, located between the first vane and the rotor (Fig. 1), indicated that at the measurement location the potential flow of the rotor had relatively small effect on the vane exit flowfield. These unsteadiness levels in velocity, as shown in Refs. 15 and 17, were of the order of 0.5% between the vane wakes and about 2% in the wakes at the midspan region, and were much smaller than the circumferential variation in the flow properties. For practical purposes, the flow at this measurement station can be considered to be steady. Thus, in the present paper, only the time-averaged data of the phase-locked average flow quantities will be discussed.

The results presented below are fully representative of the exit flowfield of an isolated annular cascade and as such allow comparison of the present mean flow data with annular cascade data obtained by previous investigators. Detailed measurements of the six components of Reynolds stresses are also shown below. Measurements of turbulence quantities have rarely been conducted in turbine cascades previously. It is hoped that these additional data will improve the understanding of the real flow effects in turbine cascades and will help both turbine designers and turbine flow modelers in developing more realistic tools for their application. The mean flow data are discussed first, followed by the turbulence data.

Mean Flow Quantities

Total Pressure Loss Coefficient

Contours of the time-averaged total pressure loss coefficients measured at station 1 are shown in Fig. 2. The flowfield is shown as it would appear to an observer looking upstream with the rotor rotating in the clockwise direction. The total pressure loss patterns are similar to ones reported previously [25, 26] in annular cascades. The loss contours appear as almost parallel lines between 20 and 60% of the span, indicating that the airfoil profile boundary layers and wakes are fairly uniform in this region. The highest losses are in the airfoil suction side hub corner where the closed contours indicate the presence of the passage vortex. The passage vortex is much weaker in the tip region than in the hub region. This is because the radial pressure gradient enhances radially inward flow, tending to spread the vortical motion over a larger area.

The loss contours over two van pitches were averaged to obtain the gap-averaged losses which are plotted below the contour plot in Fig. 2. The gap-averaged losses further illustrate the relative strength of the secondary losses in the hub and tip regions and the uniformity of the losses in the midspan regions. Also plotted in this figure are the losses obtained during a previous test using a pneumatic probe located slightly downstream of the high response probe. The data from both the pneumatic and high response probes indicate similar trends and excellent agreement in the absolute magnitude of the loss. It should be pointed out, however, that the data obtained with the high response probe were corrected for calibration drift to ensure zero loss in the inviscid region of the flowfield.

Analytical estimates of the loss generated inside the guide vane passage as obtained using the methods of Refs. 1, 27, and 28 are given in Ref. 30 and generally show good agreement with the data.

Mean Velocity Field

The three components of mean velocity at station 1 were converted to total velocity and pitch and yaw angles to clarify discussion of the data. The yaw and pitch angle data are reported in Ref. 30. The time-averaged total velocity is shown in Fig. 3 as contour plots. A comparison of contour plots in Fig. 2 and 3 indicates that the high loss regions are characterized by low total velocity. This is to be expected, because the total pressure losses are generated by viscous flows at the walls which cause retardation of the flow causing reduced velocities.

The wake centerline velocity in the midspan region is about 80% of the freestream velocity, indicating that a substantial amount of mixing has already taken place in this region. The deficit in velocity measured at the midspan wake location is in good agreement with the compressor cascade data of Raj,[29] who proposed a correlation for the decay of the cascade wake. Application of this correlation to the present data indicates that the wake centerline velocity will increase to about 95% of the freestream velocity at the rotor leading-edge plane. This implies that when the rotor airfoil passes through the wakes of this vane, it would see a negative incidence of about 2 deg. It is unlikely that such a small variation in the incidence angle would cause any substantial unsteadiness in the rotor flowfield.

The lowest velocities (60% of the freestream values) at this station are located in the center of the loss peak in the hub secondary flow region. The tip secondary flow is weaker than that near the hub both in terms of velocity and the total pressure loss. The minimum velocity in the tip region is about 70% of the freestream velocity. Experience in both plane and

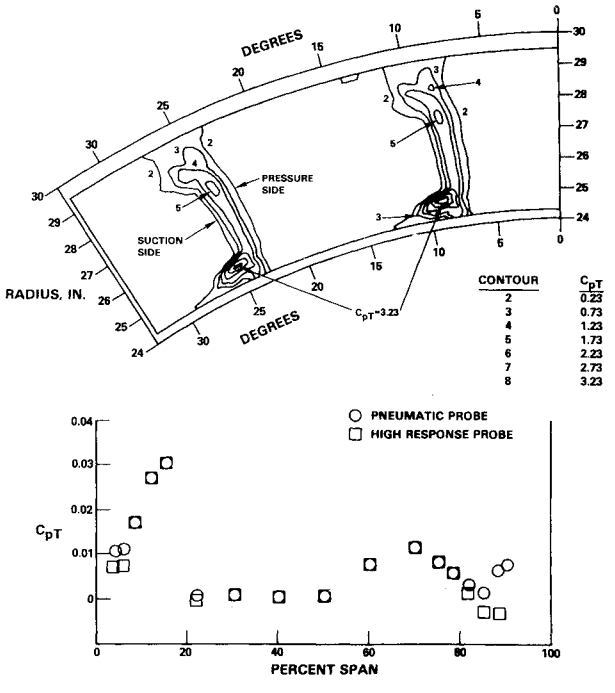

Fig. 2 Total pressure field measured at vane exit.

annular cascades indicates that secondary losses mix out at a relatively slow rate. The relatively large deficits in velocity in the secondary flow regions measured here tend to support the above experience. These unmixed secondary flow vortices are likely to persist through the rotor, and these may result in unsteadiness in the rotor flowfield.

Turbulence Intensities

The distribution of the three components of turbulence intensity are shown as contour plots in Figs. 4, 5, and 6 for the streamwise, normal, and spanwise directions, respectively. Reynolds shear stress are reported in Ref. 30. In addition, the circumferential distributions of the turbulence intensity components are shown at the hub loss peak, midspan, and tip loss peak locations. It is apparent from these figures that the turbulence intensity has very low values in the regions outside the airfoil wakes and the endwall secondary flow vortices. Of the three components of turbulence intensity at midspan, the normal component has the largest magnitudes, while the other two components are of the same order. In Ref. 18, these midspan intensities were compared with LDV measurements made in the wake of an isolated airfoil and showed good agreement for the relative distributions and order of magnitude. The turbulence intensity is almost equally distributed among the three components in the hub secondary flow vortex region.

In two-dimensional wall boundary layers, the direct production of turbulence intensity is confined to the streamwise component, which becomes the largest component of the total intensity. The transfer of energy from the streamwise to the normal and transverse components normally occurs through the fluctuating pressure velocity correlation. The presence of the wall imposes a damping in the flow, reducing in the normal component of turbulence intensity. When the flow separates at the airfoil trailing edge, the wall damping effect disappears and additional eddying caused by trailing-edge vortices results in a substantial increase in the normal component of the turbulence intensity. There are additional effects, such as wake curvature and extra rates of strain of the mean flow, which further change the distribution in the various components of turbulence intensity. The high magnitudes of the normal component of turbulence intensity in the present case is possibly due to the combination of all of the above effects.

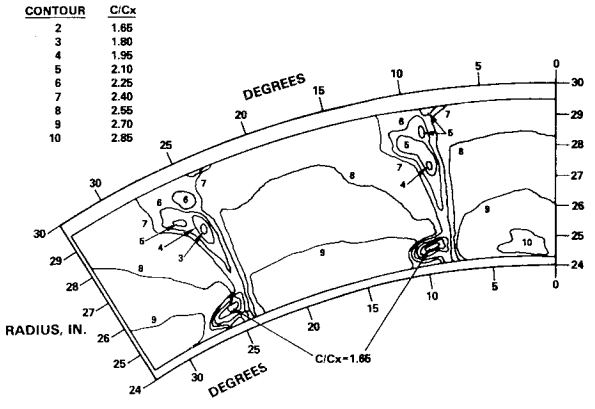

Fig. 3 Velocity magnitude measured at vane exit.

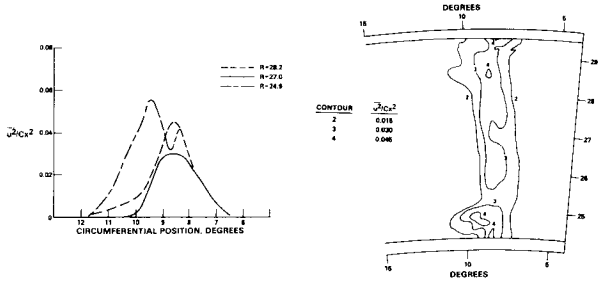

Fig. 4 Streamwise component of normal Reynolds stress measured at vane exit.

It is quite evident from the data that the turbulence field at the exit of the vanes is periodic in a manner similar to the mean flowfield. Thus, the rotor airfoils would see a substantial variation in mean and turbulence parameters when they pass through the flowfield generated by the vanes. It was pointed out previously that the mean velocity defect of the vane wakes is almost mixed out by the time the flow reaches the rotor leading edge, a least in the midspan region. The turbulence intensities, however, are likely to remain high by the time the flow reaches the rotor leading edge. This periodic variation in turbulence intensity is likely to cause substantial variation of transition location in the rotor boundary layer. Some evidence of the existence of this phenomenon was observed by Dring et al.,[17] who monitored the flowfield on the present rotor by using flush-mounted hot films. These flush-mounted hot films showed a turbulent-like boundary layer in the rotor leading-edge region when the rotor was in the vane wakes and showed laminar flow near the leading edge when the rotor was outside the vane wake regions.

Rotor Exit Flow

The measurement window in this investigation covered two first vane airfoil gaps. The number of rotor airfoils was larger (28) than that for first vane (22), thus at any given time the measurement window had flow from two vane gaps and about 2.55 rotor airfoil gaps. As a consequence of this unequal number of airfoils in the vane and the rotor rows, two adjacent airfoils in the rotor row have a different degree of interaction with the upstream vane wakes. Thus, the flowfields in the two adjacent rotor airfoil gaps cannot be directly compared.

It is appropriate, at this time, to define a nondimensional parameter that gives some indication of the degree of interaction between the rotor and the vane flowfield. This parameter is defined as:

$$S = (U_B/\tau)\ (bx/Cx)$$

where S is the reduced frequency (Strouhal number), U_B the rotor speed, τ the vane gap, bx the rotor axial chord, and Cx the throughflow velocity.

The τ/U_B in this equation represents the time it takes the rotor airfoil to traverse the upstream vane gap, and bx/Cx represents the time required for fluid particles to pass through the rotor row. The ratio of these two time scales, represented by S, gives an indication of the number of upstream wakes present in the rotor passage at any time. In the present investigation $S = 1.05$, which implies that at any time there is about one upstream wake present in the current rotor airfoil passage.

The overall flowfield downstream of the rotor at station 2 was found to be highly unsteady and more three-dimensional than the flow upstream of the rotor at station 1. In particular, the flow inside the rotor wakes and secondary flow regions was found to have large variations in the flow angles in both the circumferential and the radial directions. Because of these large angle deviations, a new hot wire reduction scheme[18] was developed to improve the angular acceptance limits of the three-sensor hot film probe. Using this new method, the angular acceptance limits were extended to the following range:

$C \pm 5\%$	$-30 \text{ deg} \le \alpha \le 40 \text{ deg}$
$\alpha \pm 3$ deg	$-25 \text{ deg} \le \beta \le 25 \text{ deg}$
$\beta \pm 3$ deg	

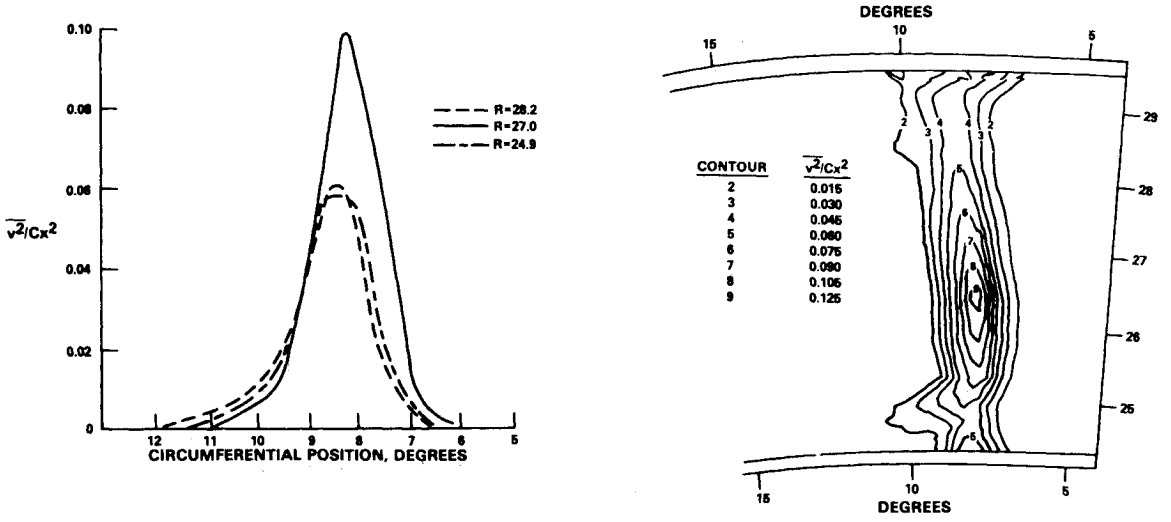

Fig. 5 Normal component of normal Reynolds stress measured at vane exit.

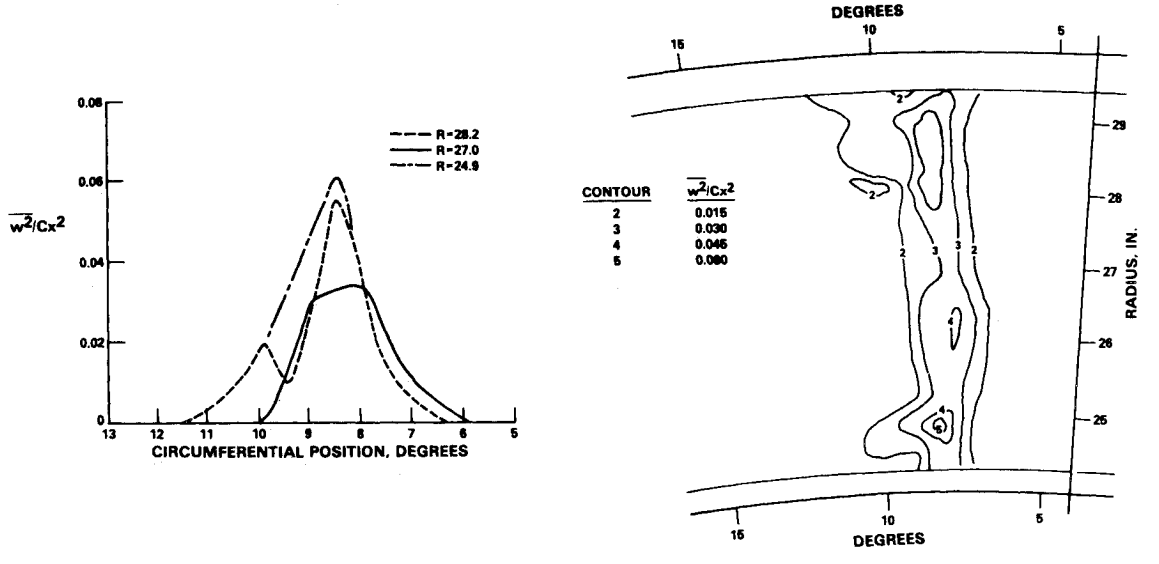

Fig. 6 Radial component of normal Reynolds stress measured at vane exit.

where C is the velocity magnitude and α and β are the pitch and the yaw angles, respectively.

These maximum inaccuracies in the velocity data occur when the flow direction approaches these outer limits of yaw and pitch angle. As the flow direction approaches $\alpha = 0$ deg and $\beta = 0$ deg, the accuracy of the data improves relative to these values. The data taken behind the rotor indicate that the regions where these outer limits are exceeded consititute a small portion of the flowfield confined to the suction side secondary flow regions. In these regions the velocity data must be interpreted only qualitatively. The accuracy of the aerodynamically shielded pressure transducer was determined to be ± 50 deg in yaw and pitch angles. Although the total pressure data are accurate over a very large angular range, comparison of the time-averaged total pressure from the high-response probe to data taken at an earlier date using a pneumatic probe showed a zero shift between the two sets of data, with the high-response probe indicating lower total pressure. These differences could not be satisfactorily resolved except that data behind the vane also showed a zero shift which could be corrected. For these reasons, the absolute levels of total pressure may be in error by the order of the zero shift (-0.23 in C_{PT}), but the gradients and relative levels of the C_{PT} contours are fairly accurate. It should be pointed out here that the total pressure drop through the rotor contains components due to both loss generation and work extraction, and as such do not give quantitative information about total pressure loss. However, low total pressure regions at this station generally occur in regions where both velocity gradients and turbulence intensities are high; thus low total pressure regions do reflect high losses rather than increased work extraction.

It was shown in the previous section that the vane exit flowfield at station 1 has two distinct regions, one dominated by the viscous wakes and vortices and the other by the potential flow. The magnitudes of turbulence intensity components in the viscous regions are much larger than in the potential flow regimes. Since the turbulence intensity decays at a slow rate, one can consider it as "marker" or "dye" of the fluid particles which, when viewed downstream of the rotor, indicates the location of the vane viscous flow. The PLA data reduction technique employed in the present investigation has allowed the flowfield downstream of the rotor to be reviewed as a function of time as the rotor airfoils move through the measurement window. The spatial and temporal variation of the turbulence intensity in the measurement window should give some clue to what happens as the upstream vane wakes and vortices pass through the rotor.

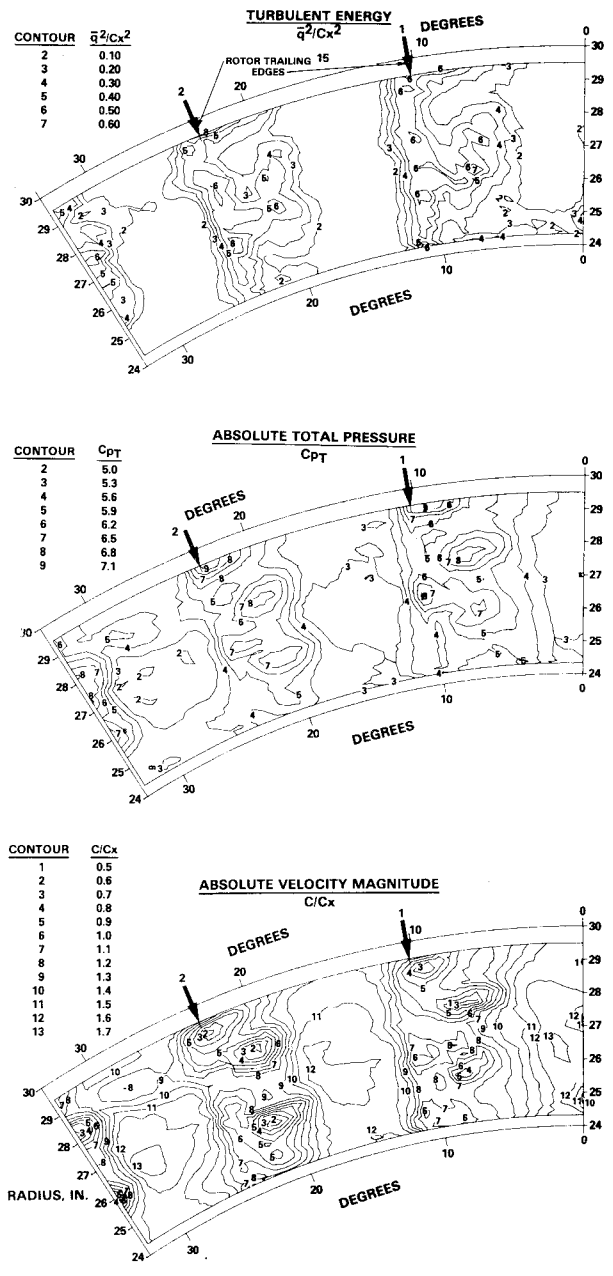

Fig. 7 Rotor exit flowfield at maximum interaction time location ($t = 20$).

A detailed review of the turbulence intensity data at station 2 obtained for 300 different locations of the rotor airfoil in the measurement window indicates the presence of two distinct flowfields representing the minimum and maximum interaction between the rotor airfoils and the vane wakes. The maximum interaction occurs at time steps $t = 20$, 120, and 220. At these time locations, one of the rotor airfoils in the measurement window is directly inside the wake of an upstream vane. Thus, all of the vane wake fluid merges with the rotor airfoil wake while the rotor midgap regions show low turbulence intensities. The turbulence intensities in the middle of the rotor airfoil gaps at these time locations are of the same order as those measured at station 1 in the potential flow region. The minimum interaction occurs at time steps $t = 80$, 180, and 280. At these time locations, the midgap regions of the rotor airfoils show large turbulence intensities. It is apparent for these time locations that the upstream vane wakes pass through the rotor gap without interacting with the rotor airfoils. The pressure, velocity, and turbulence intensity data obtained for these two time locations are described below.

Maximum Interaction $t = 20$

Figure 7 shows contour plots of the total turbulence intensity; total pressure coefficients; and mean velocity, and pitch, and yaw angles at the rotor exit in the measurement window. Static pressure and flow angles are reported in Ref. 30. The data are presented in the absolute frame of reference with the rotor moving in the clockwise direction. The suction sides of the rotor airfoil wakes appear to the right of the projection of the rotor trailing edges, which are indicated by arrow marks at the top of the contour plots.

The flow pattern in all of the contour plots in Fig. 7 shows similar behavior and exhibits two distinct regions for one rotor airfoil gap. These two regions can be identified as the potential and viscous flow regions and are discussed next.

Potential Flow Region

The flow in the gap defined by rotor airfoils 1 and 2 shows rather uniform low turbulence flow in about the middle 40% of the gap. The magnitude of turbulence intensity in this region is of the same order as that measured in the potential flow regions of the upstream vane, which indicates that the wakes and the vortices of the upstream vanes have merged with the viscous flow region of rotor airfoils 1 and 2. Flow in this region shows little variation in total and static pressures and mean velocities.

Viscous Flow Region

About 60% of the rotor airfoil gap consists of flow that is dominated by large gradients in turbulence intensity, total and static pressures, mean velocities, and pitch and yaw angles. This viscous flow region consists of the following distinct regions of flow pattern: 1) wakes, 2) tip leakage vortex, and 3) endwall secondary flow vortices.

Almost 50% of the viscous flow region shows a uniform wake structure having radial contour lines for turbulence intensity, total pressure, and mean velocities. The highest levels of turbulence velocities in this wake are of the order of about 28% of the relative freestream velocities which are much higher than those measured in the wakes of the upstream vanes. Measurement station 2 was located at about 10% axial chord downstream of the rotor trailing edge in the streamwise direction which is much closer than measurement station 1 downstream of the vane trailing edge. Measurement station 1 was located about 30% axial chord downstream of the vane trailing edge in the streamwise direction. Because of the closer proximity of station 2 to the airfoil trailing edge than that of station 1, the rotor airfoil wakes are less mixed out and contain higher turbulence intensity than those for the upstream vane.

One of the most prominent features of the rotor exit flow is the tip leakage vortex. This vortex is characterized by a very low total pressure core near each rotor airfoil tip. The tip leakage flowfield also shows low static pressure and reduced velocity magnitudes, both of which indicate the presence of high loss vortical motion in the tip region. The vortical motion in the tip leakage region data is also confirmed by the pitch and the yaw angle. A review of the data at all 300 time steps indicated that the tip leakage vortex did not seem to change in either its structure or its strength as the rotor moved through the vane flowfield.

The viscous flow between the airfoil wakes and the potential flow region is due to the endwall secondary flow vortices. These secondary flow vortices are generated in the rotor passage because of the presence of the vane exit endwall boundary layer entering the rotor, the endwall boundary layers in the rotor hub, and the tip regions and blade-to-blade pressure gradients set up by the potential flow in the midgap region. These endwall vortices, located on the suction side of the wakes, consist of low velocity, high turbulence, and low total pressure fluid. The vortices have low static pressure at their core locations, and are larger and more symmetric than

those measured at the exit of the upstream vane. The larger extent and strength of the rotor secondary flow vortices compared with those of the vane is primarily due to larger gas turning, lower acceleration, and weaker hub to tip pressure gradients in the rotor as compared to the vane. The yaw and pitch angle data confirm the presence of these two counterrotating secondary flow vortices in each rotor airfoil gap. These vortices cause overturning of the flow in the hub and the tip region, and they force the low momentum fluid to migrate toward the midspan region of the rotor airfoil suction side. Total pressure, velocity, and pitch and yaw angle data indicate that these two endwall vortices are of almost equal strength.

In summary, at this time location, the flow in the rotor airfoil gap (defined by airfoils 1 and 2) is characterized by uniform low turbulence potential flow. The fluid in the potential flow region at the rotor exit is the same fluid that left the upstream guide vane as potential flow. The fluid in the wakes and vortices of the upstream guide vane interacts with the rotor airfoil leading edge and merges with the boundary layers of the rotor airfoil pressure and suction surface. This fluid could not be distinguished from the rotor wake in the rotor exit plane. The presence of the high momentum potential flow region in the middle if the rotor airfoil gap gives rise to a strong blade-to-blade pressure gradient in the rotor passage. This strong blade-to-blade pressure gradient results in the formation of large secondary flow vortices in the rotor passage which consist of highly turbulent, low velocity and low pressure fluid. The vortical motion of this flow is confirmed by the yaw and the pitch angle measurements. The rotor exit flowfield at this time location contrasts sharply with the minmum interaction time location, which is discussed next.

Minimum Interaction $t = 80$

The minimum interaction time location is defined as the time when the upstream vane wakes and vortices pass through the rotor passages (between rotor airfoils 1 and 2 and airfoils 2 and 3) without interacting with the rotor blades.

Figure 8 shows the contour plots of the total turbulence intensity, total pressure, and mean velocity at this time location. The flow pattern shown in the figure can be divided into two regions: 1) midgap rotational flow region, and 2) viscous flow region.

Midgap "Potential/Rotational" Flow Region

The flow in the midgap regions at this time location cannot strictly be termed as potential flow because it indicates high turbulence intensity and relatively large variations in the mean velocity and total pressure. The magnitude of turbulence intensity in these regions is of the same order as in the wake and the vortices of the upstream vane, which indicates that these wakes now appear in the midgap regions between rotor airfoils 1 and 2 and airfoils 2 and 3. The average magitude of mean velocity in the midgap regions at this time location is lower than the one for time $t = 20$, which again indicates that the fluid from the upstream vane wakes is flowing in the midgap region of the rotor airfoils. Thus, we have a situation where the potential flow region of the upstream wakes interacts with the leading edge of these rotor airfoils and the wake flow forms the midchannel region. This type of a flowfield results in reduced airfoil loading and thus smaller secondary flow regimes for time $t = 80$ than the ones for time $t = 20$. Review of the viscous flow region at this time location does indicate smaller secondary flows.

Viscous Flow Region

The viscous flow region at this time location exhibits a very different structure than that for $t = 20$. The most pronounced feature of the viscous flow region is the tip leakage vortex, which is similar to the one at time $t = 80$. The secondary flow

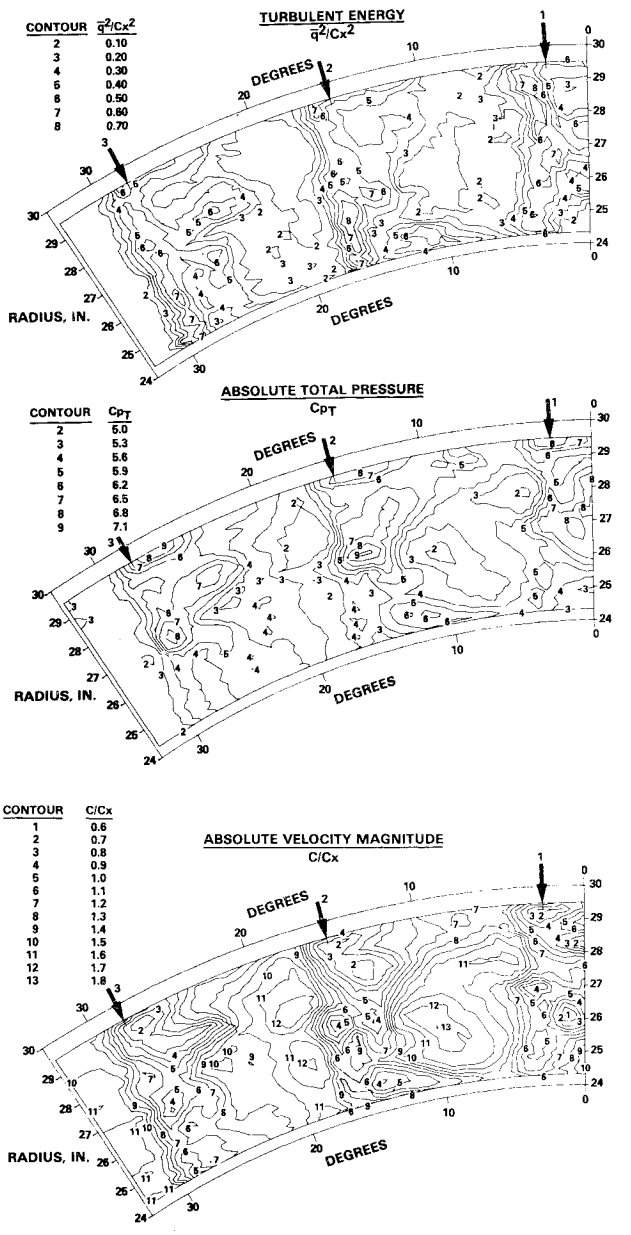

Fig. 8 Rotor exit flowfield at minimum interaction time location ($t = 80$).

regimes are more diffused and vortical motions are more spread over the entire passages at this time. The airfoil wakes look similar to the ones at $t = 20$ except that, as shown in Ref. 30, at this time location a low static pressure region exists at the midspan location almost at the center of the wake. No explanation has been postulated for the presence of this low static pressure region; however, the presence of low total pressure and low velocity fluid at its center seems to indicate that low momentum fluid may accumulate there.

In summary, for the rotor exit flow at $t = 80$, the minimum interaction time location is characterized by nonuniform inlet flow to the passages between rotors 1 and 2 and rotors 2 and 3, resulting in reduced blade-to-blade pressure gradients. This results in less intense secondary flow regions on the airfoil suction side, which are replaced by a single high-loss, low-velocity region near the wake center at midspan. This flowfield is very different from the $t = 20$ flow and is also different from the flow for the same blading tested in plane cascade.[13]

It is apparent from the above discussion that the flow downstream of the rotor is very complex. This flow is highly three-dimensional and unsteady for mean flow quantities, and it exhibits time-dependent variation in turbulence quantities.

With the acquisition of the data in the present investigation, we have barely scratched the surface of this complex flow in a turbine environment. Some concluding remarks, based on observation of this flow, are given below. Obviously, additional data and more detailed analysis are needed before a comprehensive understanding of the flowfield in a realistic turbine will emerge.

Concluding Remarks

An extensive effort was undertaken at Pratt & Whitney aimed at understanding the fundamental mechanisms governing the unsteady behavior of the flowfield in axial flow turbines. High response instrumentation and new data reduction techniques were developed to allow data with high spatial and temporal resolution to be acquired. These high resolution, high response data have allowed study of the unsteady mean and turbulent flowfield between blade rows in a large scale research turbine. The unsteady turbulence data were obtained by applying the PLA technique to the instantaneous velocity data and represent the first time such unsteady turbulence data has been acquired in a turbomachinery flowfield. The study of these data have revealed some interesting aspects of the flowfield, the impact of which is difficult to assess because of their complexity and the lack of comparable data.

Vane Exit Flow

The flowfield between the guide vane and rotor shows little effect of the downstream rotor and is essentially steady. The viscous flow at the vane exit is dominated by wakes and secondary flows and shows strong similarities to the flowfield measured for similar blading tested in annular cascade configurations. One specific contribution of this work is the detailed acquisition of turbulence data for the turbine guide vane exit flow, which, to the authors' knowledge, has not been reported previously. In the viscous flow regions significant levels of all six Reynolds stress components are present owing to the strong three-dimensionality of the mean flowfield. The turbulence data should provide insight into the interaction of the mean and turbulent flowfields in turbine cascades and will prove valuable in the development of three-dimensional calculation methods and attendant turbulence models. The large magnitudes of turbulent energy present in the viscous flow regions of the vane exit flow proved to be an effective marker of the different vane exit flow regimes, thus providing an effective experimental technique for tracking these flows through the rotor.

Rotor Exit Flow

In contrast to the vane exit flow, the flow at the rotor exit is highly unsteady and shows strong dependence on the location of the rotor airfoils relative to the upstream vane. Two flow regimes can be identified showing maximum and minimum interaction of the rotor airfoil with the upstream vane wakes.

At the maximum interaction time location, the upstream vane wakes merge with the rotor airfoil wakes, and the passage between rotor airfoils shows relatively clean low-turbulence uniform flow, while the suction side of the wake shows two large secondary-flow vortices. The overall flowfield at this location is suprisingly similar to those measured in low aspect ratio, high turning plane cascade tests. This indicates that the interaction and merging of the vane wakes with the rotor boundary layers does not significantly alter the structure of the flowfield.

At the minimum interaction time location, the upstream vane wakes pass through the rotor passage virtually without interacting with the rotor airfoils and the passage between rotor airfoils shows high-turbulence, nonuniform flow in the exit plane. The flowfield at this time location is very different from those observed in stationary cascade tests. In particular, there is no evidence of the existence of strong secondary flow vortices. In their place, a low static pressure, high loss region is present near the midspan location of the wake. The loss generation mechanisms in the flow at this time location should be very different from those in plane stationary cascades. It is important to identify and understand these mechanisms if we are to eventually control the losses in turbines.

References

[1] Dunham, J. and Came, P. M., "Improvements to the Ainley-Mathieson Method of Turbine Performance Prediction," *Journal of Engineering for Power*, Vol. 92, July 1970, pp. 252-256.

[2] Satyanarayana, B., "Unsteady Flow Past Airfoils and Cascades," Ph.D. Thesis, Cambridge University, Cambridge, U.K., 1975.

[3] Anand, A. K. and Lakshminarayana, B., "Three Dimensional Boundary Layer in a Rotating Helical Channel," *Journal of Fluids Engineering*, Vol. 97, 1975, pp. 197-210.

[4] Schmidt, D. P. and Okishi, T. H., "Multistage Axial FLow Turbomachine Wake Production, Transport and Interaction," Iowa State University, Engineering Research Institute, Ames, Rept. 77130, Nov. 1976.

[5] Hirsch, C. H. and Kool, P., "Measurement of the Three Dimensional Flow Behind and Axial Compressor Stage," *Journal of Engineering for Power*, Vol. 99, April 1977.

[6] Evans, R. L., "Boundary Layer Development on an Axial Flow Compressor Stator Blade," *Journal of Engineering for Power*, Vol. 100, April 1978, pp. 287-293.

[7] Pfeil, H. and Herbst, R., "Transition Process of Instationary Boundary Layers," ASME Paper 79-GT-128, March 1979.

[8] Pfeil, H., Herbst, R., and Schroder, T., "Investigation of the Laminar-Turbulent Transition of Boundary Layers Disturbed by Wakes," ASME Paper 82-GT-124, April 1982.

[9] Dodge, P. R., "Numerical Method for Two-Dimensional and Three-Dimensional Viscous Flows," *AIAA Journal*, Vol. 15, July 1977.

[10] Pratap, V. S., "Flow and Heat Transfer in Curved Ducts," Ph.D. Thesis, Dept. Mechanical Engineering, Imperial College, London, Aug. 1975.

[11] Briley, W. R., Kreskovsky, J. P., and McDonald, H., "Computation of Three Dimensional Viscous Flow in Straight and Curved Passages," United Technologies Research Center, E. Hartford, Conn., Rept. R76-911841-9, Aug. 1976.

[12] Hah, C., "A Navier-Stokes Analysis of Three Dimensional Turbulent Flows Inside Turbine Blade Rows at Design and Off-Design Conditions," ASME Paper 83-GT-40, 1983.

[13] Langston, L. S., Nice, M. L., and Hooper, R. M., "Three Dimensional Flow in a Turbine Cascade Passage," *Journal of Engineering for Power*, Vol. 99, Jan. 1977, pp. 21-28

[14] Marchal, P. H. and Sieverding, C. H., "Secondary Flow Within Turbomachine Bladings," *Secondary Flow in Turbomachines*, AGARD CP 214, 1977.

[15] Joslyn, H. D., Dring, R. P., and Sharma, O. P., "Unsteady Three-Dimensional Turbine Aerodynamics," ASME Paper 82-GT-161, April 1982.

[16] Dring, R. P. and Joslyn, H. D., "Measurements of Turbine Rotor Blade Flows," *Journal of Engineering for Power*, Vol. 103 April 1981, pp. 400-405.

[17] Dring, R. P., Joslyn, H. D., Hardin, L. W., and Wagner, J. H., "Turbine Rotor-Stator Interaction," ASME Paper 82-GT-3, April 1982.

[18] Butler, T. L. and Wagner, J. H., "Application of a Three Sensor Hot Wire Probe for Incompressible Flow," *AIAA Journal*, Vol. 21, May 1983, pp. 726-732.

[19] Gostelow, J. P., "A New Approach to the Experimental Study of Turbomachinery Flow Phenomenon," *Journal of Engineering for Power*, Vol. 99A, Jan. 1977, pp. 97-105.

[20] Hill, M. L. and Railly, J. W., "Time-Averaged Relative Flow Measurements by Means of an On-Line Digital Computer," Dept. of Mechanical Engineering, University of Birmingham, U. K., Research Rept. 135, Jan. 1972.

[21] Lakshminarayana, B. and Poncet, A., "A Method of Measuring Three Dimensional Rotating Wakes Behind Turbomachinery Rows," *Journal of Fluids Engineering*, Vol. 96, June 1974, pp. 87-91.

[22] Gorton, C. A. and Lakshminarayana, B., "A Method of Measuring the Three Dimensional Mean Flow and Turbulence

Quantities Inside a Rotating Turbomachinery Passage," *Journal of Engineering for Power*, Vol. 98, April 1976, pp. 137-146.

[23] Squire, H. B. and Winter, K. G., "The Secondary Flow in a Cascade of Airfoils in a Nonuniform Stream," *Journal of the Aeronautical Sciences*, Vol. 18, 1951.

[24] Hawthorne, W. R., "Secondary Circulation of Fluid Flow," *Proceedings of the Royal Society of London*, Vol. 206, May 1951, pp. 374-387.

[25] Rohlick, H. E., Allen, H. W., and Herzig, H. W., "Study of the Secondary Flow Patterns in an Annular Cascade of Turbine Nozzle Blades," NACA TN 2909, Dec. 1953.

[26] Hunter, I. H., "Endwall Boundary Layer Flows and Losses in Axial Turbomachines," Ph.D. Thesis, Cambridge University, U.K., 1979.

[27] Sharma, O. P. and Graziani, R. A., "Influence of Endwall Flow on Airfoil Suction Surface Mid-Height Boundary Layer Development," *Journal of Engineering for Power*, Vol. 105, Jan. 1983, pp. 147-155.

[28] Mukhtarov and Krichakin, "Procedure for Estimating Flow Section Losses in Axial Flow Turbines when Calculating Their Characteristics," *Teploenergetika*, Vol. 18, 1969, pp. 76-79.

[29] Raj, R., "On the Investigation of Cascade and Turbomachinery Rotor Wake Characteristics," Ph.D. Thesis, Dept. Aerospace Engineering, Pennsylvania State University, University Park, Pa., 1974.

[30] Sharma, O. P., Butler, T. L., Joslyn, H. D., and Dring, R. P. "An Experimental Investigation of the Three Dimensional Unsteady Flow in an Axial Flow Turbine," AIAA Paper 83-1170, June 1983.